Biomedical Research (Tokyo) **47** (1) 11–23, 2026

Tenascin-XB plays a role in the infiltration of immune cells in tumor microenvironment

Ao Gong[1], Yuichi Iida[2], Kohei Kawakami[3], Kazuo Yamada[1], Yasuyuki Saito[2], and Ken-ichi Matsumoto[1]

[1] Department of Biosignaling and Radioisotope Experiment, Interdisciplinary Center for Science Research, Head Office for Research and Academic Information, Shimane University, 89-1 Enya-cho, Izumo 693-8501, Japan; [2] Department of Immunology, Shimane University Faculty of Medicine, 89-1 Enya-cho, Izumo 693-8501, Japan; and [3] Department of Experimental Animals, Interdisciplinary Center for Science Research, Head Office for Research and Academic Information, Shimane University, 89-1 Enya-cho, Izumo 693-8501, Japan

(Received 23 October2025; and accepted 28 October2025)

ABSTRACT

We previously showed that tenascin-XB (TNXB) contributes to tumor suppressor function. The present study aimed to assess the tumor-suppressive mechanism of TNXB by focusing on immune cell infiltration into the tumor microenvironment (TME). We revealed that B16-OVA melanoma cells (MO5)-bearing TNXB-deficient (*Tnxb*$^{-/-}$) mice exhibited significant tumor progression and a poor survival rate. Allogeneic mixed lymphocyte reaction showed reduced numbers and increased activation of both CD4$^+$ and CD8$^+$ T cells from *Tnxb*$^{-/-}$ spleens. Moreover, T cell activation assay further proved that CD4$^+$ and CD8$^+$ T cells from *Tnxb*$^{-/-}$ mice were more activated than those from WT mice. RT-qPCR analysis showed that expression of T cell activation-related cytokines and chemokines was significantly decreased in tumor tissues from *Tnxb*$^{-/-}$ mice. Flow cytometry analysis revealed a reduced infiltration level of CD8$^+$ T cells in both naïve spleens and tumor tissues in *Tnxb*$^{-/-}$ mice. Ultimately, total activation of CD8$^+$ T cells was decreased in tumor tissues in *Tnxb*$^{-/-}$ mice. In conclusion, we found that although *Tnxb*$^{-/-}$ CD4$^+$ and CD8$^+$ T cells tend to be activated more than WT CD4$^+$ and CD8$^+$ T cells, CD8$^+$ T cell infiltration and activation level were attenuated in tumor sites of *Tnxb*$^{-/-}$ mice.

Keywords: Extracellular matrix glycoprotein, tenascin-XB, tumor-bearing mice, tumor microenvironment, T cell infiltration, Ehlers-Danlos syndrome

Address correspondence to:
Ken-ichi Matsumoto, Ph.D.
Department of Biosignaling and Radioisotope Experiment, Interdisciplinary Center for Science Research, Head Office for Research and Academic Information, Shimane University, 89-1 Enya-cho, Izumo 693-8501, Japan
Tel: +81-853-20-2248, Fax: +81-853-20-2248
E-mail: matumoto@med.shimane-u.ac.jp

Yuichi Iida, Ph.D.
Department of Immunology, Shimane University Faculty of Medicine, 89-1 Enya-cho, Izumo 693-8501, Japan
Tel: +81-853-20-2690, Fax: +81-853-20-2459
E-mail: yiida@med.shimane-u.ac.jp

INTRODUCTION

The tumor microenvironment (TME) comprises numerous cell types besides tumor cells, including immune cells, fibroblasts, blood vessels, and extracellular matrix (ECM) (Hanahan *et al.* 2012). These cells secrete tumor-specific ECMs, cytokines, growth factors, and matrix remodeling enzyme, such as matrix metalloproteinases (MMPs). The ECMs surrounding the tumor cells contribute to the progression, apoptosis, metastasis, and immune suppression of embedded tumor cells (Pickup *et al.* 2014). Tenascins are a family of large, multifunctional glycoproteins of the ECM consisting of four members (tenascin-C, -R, -XB, and -W) (Chiquet-Ehrismann

et al. 2011). Tenascin-C (TNC) and Tenascin-W (TNW) are specifically present in various tumor stroma, while they are localized with relatively low abundance in normal tissues (Brellier *et al.* 2012). TNC and TNW have been promised as targets for anti-cancer therapies (Spenlé *et al.* 2015; Tucker *et al.* 2019).

Tenascin-XB (TNXB) is involved in collagen deposition, collagen stability, and collagen fibrillogenesis (Valcourt *et al.* 2015; Okuda-Ashitaka *et al.* 2023). TNXB deficiency by homozygous or compound heterozygous pathogenic variants in the *TNXB* gene causes a heritable connective tissue disorder called classical-like Ehlers-Danlos syndrome type 1 (clEDS1) (Malfait *et al.* 2020). Patients diagnosed with clEDS1 show velvety smooth skin, hyperextensible skin without atrophic scarring, joint hyperflexibility, deformities of the hands and feet, and easy bruising (Demirdas *et al.* 2017). However, in tumor-related areas, there are few reports on TNXB, except for its expression patterns in various tumor tissues. *TNXB* expression is significantly downregulated during tumor progression in most tumor tissues (Chakravarthy *et al.* 2018), and high expression of *TNXB* is positively correlated with good prognosis (Liot *et al.* 2020). Previously, we demonstrated that B16-BL6 melanoma-bearing *Tnxb*$^{-/-}$ mice exhibited prominent proliferation of melanoma cells and an increase in invasion and metastasis, which were caused by enhanced activities and expression of MMPs compared with those of their melanoma-bearing WT mice (Matsumoto *et al.* 2001). We also revealed by *in vitro* experiments that the induction of *Mmp2* in *Tnxb*-deficient fibroblasts is mediated through c-Jun N-terminal kinase (JNK) and protein tyrosine kinase phosphorylation pathways (Matsumoto *et al.* 2004). Furthermore, *in vitro* knockdown and knockout experiments of *TNXB* in esophageal squamous cell carcinoma (ESCC) showed enhanced cell proliferation and colony formation (Yang *et al.* 2020). These data suggest that TNXB functions as a tumor suppressor (Okuda-Ashitaka *et al.* 2023). However, the role of TNXB in TME remains obscure.

The ECM influences anti-tumor immunity by modulating the localization and migration of immune cells (Eble *et al.* 2019). CD8$^+$ T cells are preferentially present in the stromal regions with a looser network of fibronectin and collagen (Salmon *et al.* 2012). High collagen-density reduces the number of infiltrating CD8$^+$ T cells and their cytotoxic activity, while increasing the number of regulatory T cells (Tregs) in tumor tissues (Kuczek *et al.* 2019). Interestingly, TNC retains infiltrated CD8$^+$ T cells via TNC/CXCL12/CXCR4 (Murdamoothoo *et al.* 2021) and TNC/CCL21/CCR7 (Spenlé *et al.* 2020) pathways in the TNC-rich stroma, leading to the progression of tumor nests.

In the present study, to investigate the tumor suppressive mechanism of TNXB, especially focusing on the infiltration of immune cells within the TME, we created the B16-OVA melanoma cells (MO5)-bearing *Tnxb*$^{-/-}$ mice and examined the infiltration and activation of T cells in the TME. We found that TNXB deficiency facilitated tumor progression by reducing CD8$^+$ T cell infiltration with decreased activation *in vivo*, indicating that TNXB deficiency creates poor immune response in TME. Therefore, TNXB may serve as a novel immunotherapeutic target for suppressing tumor progression.

MATERIALS AND METHODS

Mice. Six-week-old C57BL/6 (WT) and BALB/c female mice were obtained from CLEA Japan Inc. (Tokyo, Japan), and TNXB-deficient mice (*Tnxb*$^{-/-}$) were generated by homologous recombination using embryonic stem cells (Matsumoto *et al.* 2001). *Tnxb*$^{-/-}$ mice were established by backcrossing into a congenic line, C57BL/6 (Matsumoto *et al.* 2004). All mice were maintained under specific pathogen-free conditions (SPF) with free access to food and water at Shimane University. All animal experiments were approved by the Ethical Committee for Animal Research of Shimane University (IZ5-59-1, IZ5-59-2) and followed ethical guidelines.

Cell culture. B16-OVA melanoma cells (MO5) (Sigma-Aldrich, St. Louis, MO, USA) were maintained in RPMI-1640 medium (Sigma-Aldrich) supplemented with 10% fetal bovine serum (FBS) (Sigma-Aldrich) and 20 μg/mL gentamicin (Nacalai Tesque, Kyoto, Japan).

In vivo tumor growth experiment. B16-OVA melanoma cells (MO5) (1×10^6) were subcutaneously (s.c.) inoculated into the right flank of WT and *Tnxb*$^{-/-}$ mice. Twelve days after tumor inoculation, tumor volume (mm^3, $V = \frac{L \times W^2}{2}$, L: length, W: width) was measured with digital vernier calipers every 2 days, and 80 mm^3 tumor volume (cut-off volume) were used for tumor growth analysis. Lungs were harvested and processed for tumor metastasis analysis after death. The Kaplan-Meier (KM) method was

used to estimate the survival rate and plot the survival curve after tumor inoculation.

T cell isolation by nylon wool fiber. Nylon wool fiber (NWF, 0.6 g) (Cosmo Bio Company, Tokyo, Japan) was placed in a 10 mL syringe and autoclaved. The syringe was set with a three-way stopcock and incubated with RPMI-1640 medium with 10% FBS at 37°C in 5% CO_2 for 1 h. Cell suspension [Nyron wool fiber treatment (−) and NWF(−) as indicated in Fig. 2] of the spleens was prepared as described below and then added to the syringe. The stopcock was closed until the splenocytes trespassed into the packed wool. Additional medium (5 mL) was added to the syringe to cover the wool fiber and incubated at 37°C in 5% CO_2 for 1 h. Finally, the T cell suspension [Nyron wool fiber treatment (+) and NWF(+) as indicated in Fig. 2] was collected in a fraction that passed through the nylon wool fiber.

T cell enrichment. Surface staining of the enriched T cells was conducted using the following antibodies: anti-CD3ε (clone 145-2C11; BioLegend, San Diego, CA, USA), anti-CD19 (clone 6D5, BioLegend). Flow cytometry was conducted using CytoFLEX (Beckman Coulter, Brea, CA, USA).

In vitro allogeneic mixed lymphocyte reaction (allo-MLR). Spleens were harvested from WT, *Tnxb*$^{-/-}$, and BALB/c female mice, then mashed with frosted slides in PBS and filtered through a gauze mesh. The cell suspension was centrifuged at 430 ×*g* for 3 min and resuspended in 5 mL of RBC lysis solution (Thermo Fisher Scientific, Waltham, MA, USA) to lyse the red blood cells. The cells were maintained in RPMI-1640 medium with 10% FBS. BALB/c mice-derived splenocytes (allogeneic cells) as a stimulator were treated with 50 μg/mL mitomycin C (MMC) (Nacalai Tesque) for 2 h at 37°C to inhibit cell growth and division, and then co-cultured with either splenocytes of WT or *Tnxb*$^{-/-}$ mice at a 4 : 1 cell number ratio for 96 h. For flow cytometry analysis, cells were washed with FACS buffer (1% FBS in PBS) and pre-stained with Zombie NIR™ Fixable Viability Kit (Biolegend) at room temperature in the dark for 30 min. Cells were stained with the following antibodies: anti-H-2Kd (clone SF1-1.1, BioLegend), anti-TCRβ (clone H57-597, BioLegend), anti-CD4 (clone GK1.5, BioLegend), anti-CD8α (clone 53-6.7, BioLegend), and anti-CD69 (clone H1.2F3, BioLegend). Flow cytometry was conducted using CytoFLEX.

In vitro T cell activation assay by phorbol myristate acetate (PMA) and ionomycin. To measure T cell activation, splenocytes were obtained from WT and *Tnxb*$^{-/-}$ mice, followed by mashing, filtration, and lysis of red blood cells, as described above. Splenocytes were then washed with PBS and seeded in 6-well plates with equal cell numbers (5.0×10^6 cells/well) in a total volume of 2 mL RPMI-1640 medium with 10% FBS and stimulated with 40 ng/mL phorbol myristate acetate (PMA) (Thermo Fisher Scientific) and 4 μg/mL ionomycin (Thermo Fisher Scientific) for 4 h and 24 h, respectively. Cells were then detached and washed with 2 mL of FACS buffer, and cell surface staining was conducted using the following antibodies: anti-CD44 (clone IM7, BioLegend), anti-CD62L (clone MEL-14, BioLegend), anti-CD4, and anti-CD8α. Flow cytometry was conducted using CytoFLEX.

Analysis of T cell infiltration in naïve spleens and tumor tissues from tumor-bearing mice. Naïve spleens and tumor tissues from tumor-bearing mice after tumor inoculation for 12 days were harvested from WT and *Tnxb*$^{-/-}$ mice, and a cell suspension was prepared as described above. The cells were then washed with the FACS buffer. Tumor cells were pre-stained with the Zombie NIR™ Fixable Viability Kit (Biolegend) at room temperature in the dark for 30 min before cell surface staining. Cell surface staining was conducted using the following antibodies: anti-CD3ε, anti-CD45 (clone 30-F11, BioLegend), anti-CD4, anti-CD8α, anti-TCRβ, and anti-CD69. Flow cytometry was conducted using CytoFLEX.

ELISA. Splenocytes from WT and *Tnxb*$^{-/-}$ mice were obtained and maintained as described above. The cells were then stimulated with 40 ng/mL of PMA and 4 μg/mL of ionomycin for 24 h, 48 h, 72 h, and 96 h, respectively, followed by collection of the supernatants. IFN-γ concentration was measured by IFN gamma Standard ELISA Development Kit (PeproTech, Cranbury, NJ, USA). Absorbance was measured at 450 nm using a GloMax Discover Microplate Reader (Promega Corporation, Madison, WI, USA).

Reverse transcription-quantitative PCR (RT-qPCR). Total RNA was isolated from the naïve spleens, T cell-enriched fraction of naïve spleens, and spleens and tumor tissues of tumor-bearing WT and *Tnxb*$^{-/-}$ mice using the ISOSPIN Cell & Tissue RNA Kit (Nippon Gene Co., Ltd., Tokyo, Japan) according to the manufacturer's instructions. cDNA was synthe-

sized from 1 μg of RNA using PrimeScript RT Reagent Kit (Takara Bio Inc., Shiga, Japan) and the T100 Thermal Cycler (Bio-Rad, Hercules, CA, USA). The synthesized cDNA was subjected to quantitative PCR (qPCR) using TB Green Premix Ex Taq II (Takara Bio Inc.) on a Thermal Cycler Dice Real Time System II TP900 (Takara). *Actb* was used as the internal control. Relative expression was calculated using the $2^{-\Delta\Delta Cq}$ method with normalization to *Actb* (Livak *et al.* 2001).

The following primer sequences were used : *Tnf*, (forward) 5′-CCCTCACACTCAGATCATCTTCT-3′ and (reverse) 5′-GCTACGACGTGGGCTACAG-3′; *Il2*, (forward) 5′-GATGAACTTGGACCTCTGCG-3’ and (reverse) 5′-CATCATCGAATTGGCACTCA-3′; *Il7*, (forward) 5′-CTGATGATCAGCATCGATGAA TTGG-3′ and (reverse) 5′-GCAGCACGATTTAGA AAAGCAGCTT-3′; *Cxcl9*, (forward) 5′-GAGCAG TGTGGAGTTCGAGG-3′ and (reverse) 5′-TCCG GATCTAGGCAGGTTTG-3′; *Cxcl10*, (forward) 5′-CCAAGTGCTGCCGTCATTTTC-3′ and (reverse) 5’-GGCTCGCAGGGATGATTTCAA-3′; *Cxcl11*, (forward) 5′-AACAGGAAGGTCACAGCCAT-3′ and (reverse) 5′-GCTTTCTCGATCTCTGCCAT-3′; *Tnxb*, (forward) 5′-ATTCTCTCCTCGGTCTAA TG-3′ and (reverse) 5′-GGGTGAACACCACCTGC TTC-3′; *Actb*, (forward) 5′-GACCTCTATGCCAAC ACAGT-3′ and (reverse) 5′-GATCTTCATGGTGCT AGGAG-3′. The primers used for the Supplementary Fig. 2 are listed in Supplementary Table 1.

Immunofluorescence analysis. Tumor tissues were harvested, embedded in optimal cutting temperature (OCT) compound (Sakura Finetek USA, Inc., Torrance, CA, USA), flash-frozen, and sectioned into 6-μm-thick pieces using a cryostat (Leica, Wetzlar, Germany). For immunofluorescence staining, sections were air-dried at room temperature for 30 min, fixed with 4% paraformaldehyde (PFA) (Nacalai Tesque) for 10 min, and blocked in 10% goat serum for 1 h (Immuno-Biological Laboratories Co., Ltd., Fujioka, Gunma, Japan). Subsequently, sections were incubated overnight at 4°C with primary antibody (1 : 100), followed by incubation for 1 h at room temperature with secondary antibody (1 : 1000). Finally, the sections were mounted with ProLong Gold Antifade with DAPI (Cell Signaling Technology, Danvers, MA, USA) and sealed with a coverslip surrounded by nail polish. Images were processed using an FV3000 confocal microscope (Olympus, Tokyo, Japan). The following primary antibodies were used: anti-TNXB (pAbM23, anti-rabbit) (Matsumoto *et al.* 2006), anti-CD4 (clone GK1.5, anti-rat, BioLegend), anti-CD8α (clone 5H10-1; anti-rat, BioLegend). The following secondary antibodies were used: Alexa Fluor 488-conjugated goat anti-rabbit antibody (Cell Signaling Technology, #4412), Alexa Fluor 555-conjugated goat anti-rat antibody (Cell Signaling Technology, #4417), and Alexa Fluor 647-conjugated goat anti-rat antibody (Cell Signaling Technology, #4418).

Statistical analysis. GraphPad Prism (version 10.1.2) software was used for the statistical analysis and the Kaplan-Meier (KM) curve graphing. A two-tailed unpaired *t*-test of variance and a two-way ANOVA with uncorrected Fisher’s Least Significant Difference (LSD) test were used for two-group analysis. Ordinary one-way ANOVA followed by the Tukey test was used for multi-group analysis. $P < 0.05$ was considered statistically significant. $*P < 0.05$; $**P < 0.01$; $***P < 0.001$; $****P < 0.0001$; ns, not significant.

RESULTS

Significant tumor growth in $Tnxb^{-/-}$ mice after inoculation of B16-OVA melanoma cells (MO5)

Previously, we demonstrated that tumor invasion and metastasis were promoted after the inoculation of B16-Bl6 melanoma cells into the footpad of $Tnxb^{-/-}$ mice (Matsumoto *et al.* 2001). First, to confirm the results of our previous study, we examined the growth of other melanoma cells, B16-OVA melanoma cells (MO5), which were subcutaneously inoculated into the right flank of WT and $Tnxb^{-/-}$ mice. As shown in Fig. 1A, tumor growth was significantly increased in $Tnxb^{-/-}$ mice than in WT mice. In addition, overall survival rates were reduced in $Tnxb^{-/-}$ mice than those in WT mice (Fig. 1B). To assess poor survival, we investigated pulmonary metastasis; however, metastasis was not detected (data not shown).

T cells themself do not express Tnxb

Tnxb expression is prominently in connective tissue (Geffrotin *et al.* 1995). However, its expression in T cells has not yet been explored. To investigate *Tnxb* expression in T cells, we enriched T cells from naïve spleens with nylon wool fiber. Anti-CD19 and anti-CD3ε antibodies were used for B cell and T cell determination, respectively. Enriched T cells were defined as $CD3^+$ $CD19^-$ (Fig. 2A). Following the purification of RNA from total spleen extract [Nyron wool fiber treatment (−) and NWF(−) as indicated in Fig. 2] and T cell-enriched fraction [Nyron

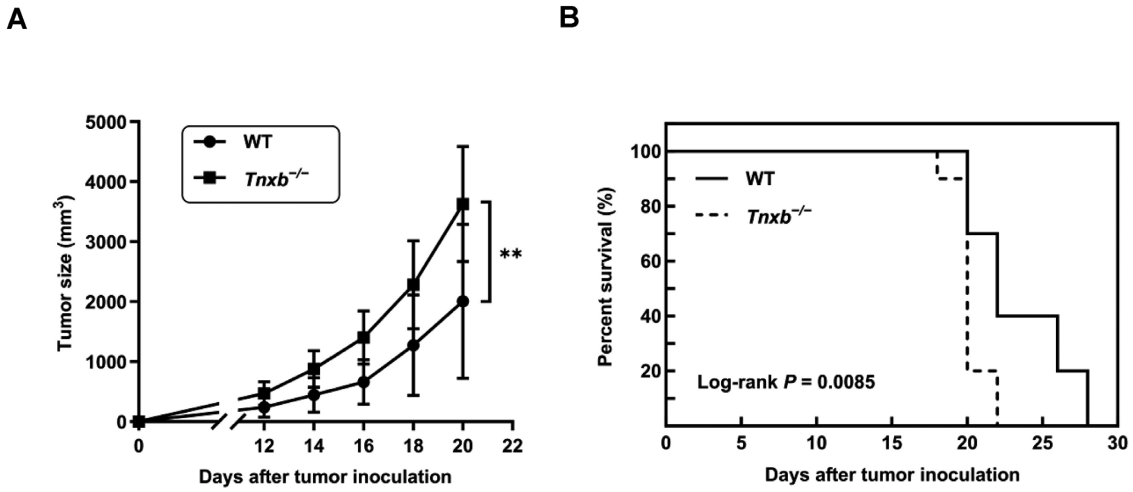

Fig. 1 *Tnxb*$^{-/-}$ mice exhibit increased tumor growth and a poor survival rate. (**A**) Twelve days after tumor inoculation, the tumor size (mm^3) was measured every 2 days. Each group contained ten mice ($n = 10$). Data are expressed as the mean ± SD (**$P < 0.01$, two-tailed unpaired *t*-test). (**B**) A Kaplan-Meier (KM) curve was drawn to estimate the survival rate of WT and *Tnxb*$^{-/-}$ mice.

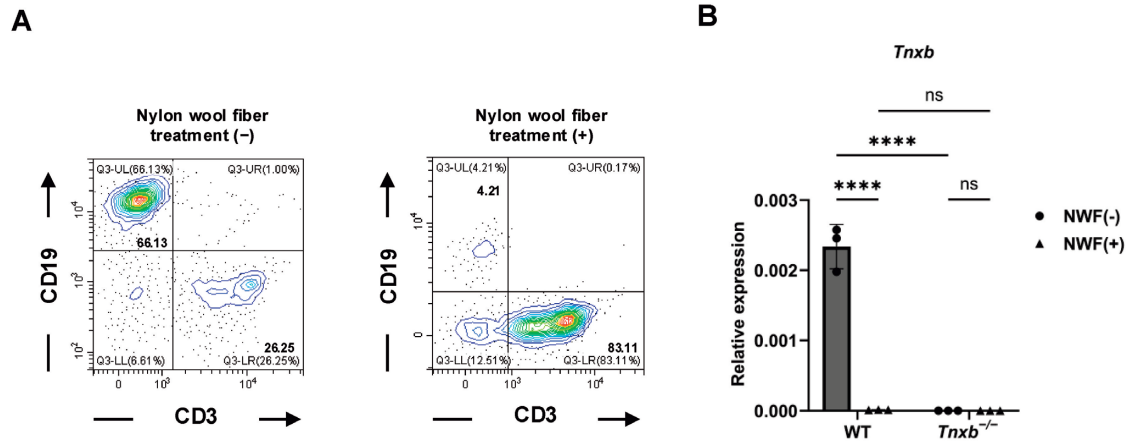

Fig. 2 T cells themselves do not express *Tnxb*. The T cell population from spleen was enriched after nylon wool fiber treatment. (**A**) Representative contour plots showing T cell population of naïve splenocytes before (left) [Nylon wool fiber treatment (–)] and after nylon wool fiber (NWF) treatment (right) [Nylon wool fiber treatment (+)]. CD19 and CD3 were used for B cell and T cell identification, respectively, and enriched T cells were defined as CD3$^+$ CD19$^-$. (**B**) Expression of *Tnxb* in T cells from the spleens of WT and *Tnxb*$^{-/-}$ mice with (+) or without (–) NWF treatment. Expression of *Tnxb* in each fraction was investigated by RT-qPCR. Data were normalized to *Actb*. Each group consisted of three mice ($n = 3$). Data are presented as mean ± SD (****$P < 0.0001$; ns, not significant; two-way ANOVA with uncorrected Fisher's LSD test).

wool fiber treatment (+) and NWF(+) as indicated in Fig. 2], *Tnxb* expression was investigated by RT-qPCR. We found that the enriched T cells did not express *Tnxb*, indicating that the cells expressing *Tnxb* were not T cells (Fig. 2B). In addition, we searched CZ CELLxGENE Discover single cell database (https://cellxgene.cziscience.com) to identify the possible *Tnxb*-expressed cells in spleen. As shown in Supplementary Fig. 1, we found that *Tnxb* is mainly expressed in myeloid leukocytes, macrophages, and myeloid cells but not in various types of T cells.

Both CD4$^+$ and CD8$^+$ T cell populations were decreased in Tnxb$^{-/-}$ *splenocytes, but Tnxb*$^{-/-}$ *T cells exhibited higher activation levels compared to WT T cells*

We subsequently investigated whether TNXB deficiency affects the T cell proliferation and activation, especially in CD4$^+$ and CD8$^+$ T cells. We performed

the allo-MLR experiments *in vitro* in a cell culture system. MMC-treated splenocytes from BALB/c mice were co-cultured with WT or *Tnxb*$^{-/-}$ splenocytes. We evaluated WT and *Tnxb*$^{-/-}$ T cell activation by CD69 expression. CD4$^+$ and CD8$^+$ T cells were defined as TCRβ$^+$ CD4$^+$ and TCRβ$^+$ CD8$^+$, respectively, after gating on H-2Kd$^-$ cells. Activated CD4$^+$ and CD8$^+$ T cells were defined as CD69$^+$ CD4$^+$ and CD69$^+$ CD8$^+$, respectively, after gating on H-2Kd$^-$ TCRβ$^+$ cells. We found significantly lower proliferation of CD4$^+$ and CD8$^+$ T cells from *Tnxb*$^{-/-}$ mice than those from WT mice after stimulation (Fig. 3A and B). Unstimulated CD8$^+$ T cells from *Tnxb*$^{-/-}$ mice exhibited less amount of proliferation than those from WT mice (Fig. 3B). Meanwhile, compared with WT mice, the activation of CD4$^+$ cells from *Tnxb*$^{-/-}$ mice, detected as CD69$^+$ cells, was significantly increased (Fig. 3C). However, the activation of CD8$^+$ cells from *Tnxb*$^{-/-}$ mice tended to be increased but not significantly compared with those from WT mice (Fig. 3D).

To further examine whether T cell activation is affected by TNXB deficiency, we stimulated CD4$^+$ and CD8$^+$ T cells from splenocytes with PMA and ionomycin *in vitro* in a cell culture system. Naïve and effector memory T cells (T_{EM}) were defined as CD44$^-$ CD62L$^+$ and CD44$^+$ CD62L$^-$, respectively, after gating on TCRβ$^+$ CD4$^+$ or TCRβ$^+$ CD8$^+$ T cells (Fig. 4A and B). Without stimulation, most CD4$^+$ and CD8$^+$ T cells were naïve (Fig. 4A and B). Furthermore, the naïve CD8$^+$ T cell population was lower in *Tnxb*$^{-/-}$ than in WT mice (Fig. 4B and D), while the naïve CD4$^+$ T cell population was higher in *Tnxb*$^{-/-}$ than in WT mice (Fig. 4A and C). In contrast, without stimulation, CD4$^+$ and CD8$^+$ T_{EM} subsets from *Tnxb*$^{-/-}$ spleens were lower than those from WT mice (Fig. 4C and D). To evaluate the frequency of activation, the effector memory population after stimulation was normalized to that of unstimulated controls. The resulting frequency of CD44$^+$ CD62L$^-$ CD4$^+$ T_{EM} from *Tnxb*$^{-/-}$ mice was significantly higher than those from WT mice after stimulation for 20 h (Fig. 4E). In contrast, the frequency of CD44$^+$ CD62L$^-$ CD8$^+$ T_{EM} from *Tnxb*$^{-/-}$ mice was significantly higher than those from WT mice after stimulation for 4 h and 20 h (Fig. 4F). Contrary to our expectation, *Tnxb*$^{-/-}$ CD4$^+$ and CD8$^+$ T cells exhibited greater activation than WT following *in vitro* stimulation.

T cell activation-related cytokines and chemokines were downregulated in tumor tissues of Tnxb$^{-/-}$ *mice*

To investigate the mechanism underlying TNXB deficiency-induced tumor progression, we examined the expression of T cell activation-related cytokines and chemokines and immune-related genes in WT and *Tnxb*$^{-/-}$ mice. Initially, in the naïve spleens, *Tnxb*$^{-/-}$ mice exhibited significantly decreased expression of *Tnf* and *Cxcl9* involved in immune inflammation and activation (Fig. 5A), while the expression of *Pdcd1* and *Ctla4,* involved in T cell exhaustion, and *Ly6g,* involved in myeloid-derived suppressive cells (MDSCs), were increased (Supplementary Fig. 2A), indicating that TNXB deficiency intrinsically contributes to poor immune response in TME. The levels of cytokines *Il2* and *Il7* and chemokines *Cxcl10*, *Cxcl11*, *Ccl17*, and *Ccl22* in the naïve spleens were not significantly different between WT and *Tnxb*$^{-/-}$ mice (Fig. 5A and Supplementary Fig. 2A). After tumor inoculation, at day 12, spleens of tumor-bearing mice showed similar results except for *Cxcl9* expression (Fig. 5B and Supplementary Fig. 2B). Finally, in the tumor tissues after tumor inoculation for 12 days, the expression of T cell activation-related cytokines and chemokines *Il2, Il7, Cxcl9,* and *Cxcl10* and *Tnf* were significantly decreased in the *Tnxb*$^{-/-}$ mice (Fig. 5C). While the expression of *Ly6g* was increased, that of chemokine *Ccl22* was decreased in the *Tnxb*$^{-/-}$ mice (Supplementary Fig. 2C). The expression of *Pdcd1*, *Ctla4* and *Ccl17* was not significantly different between WT and *Tnxb*$^{-/-}$ mice (Supplementary Fig. 2C). These results indicate that TNXB deficiency contributes to the downregulation of T cell activation-related cytokines and chemokines, whereas the upregulation of MDSC marker, particularly within tumor tissues, may facilitate tumor progression.

We also investigated the IFN-γ concentration in the cell culture supernatant of splenocyte after PMA and ionomycin stimulation. IFN-γ concentration was significantly lower in the cell culture supernatant of *Tnxb*$^{-/-}$ mice than that of WT mice after the stimulation for 24 h and 48 h, but not significant after stimulation for 72 h and 96 h (Fig. 5D). Interestingly, although CD4$^+$ and CD8$^+$ T cells from *Tnxb*$^{-/-}$ mice were greatly activated than those from WT mice after stimulation (Fig. 4E and F), the anti-tumor effect of the immune cells from *Tnxb*$^{-/-}$ mice by IFN-γ was weaker than those from WT mice *in vitro* (Fig. 5D).

TNXB deficiency reduced CD8$^+$ T cell infiltration and activation in tumor tissues in vivo

We investigated the infiltration and activation of CD4$^+$ and CD8$^+$ T cells in both naïve spleens (Supplementary Fig. 3) and tumor tissues from WT and *Tnxb*$^{-/-}$ mice *in vivo* after tumor inoculation for 12

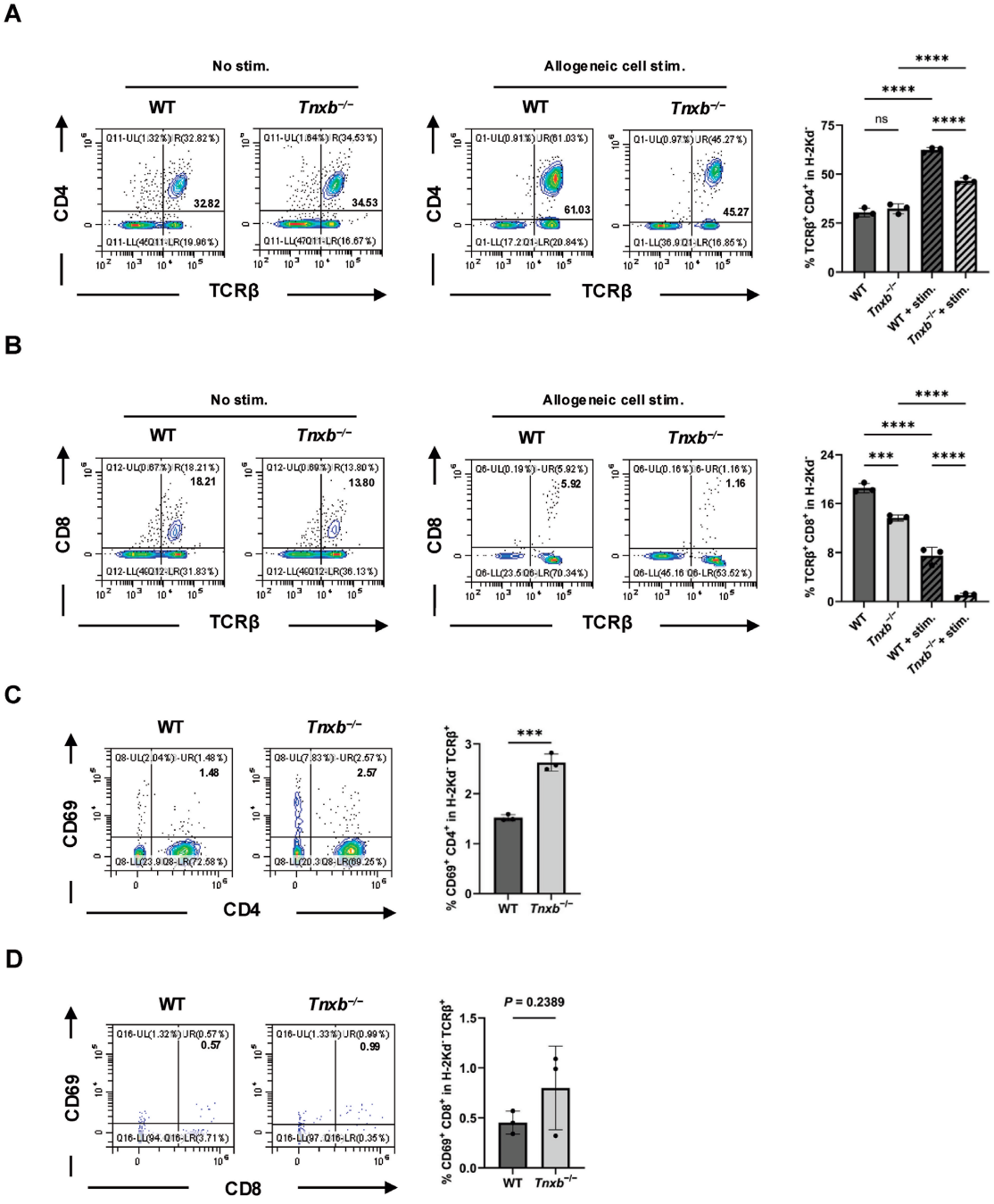

Fig. 3 *Tnxb*$^{-/-}$ CD4$^+$ and CD8$^+$ T cells exhibit reduced cell populations but increased activation after stimulation with allogeneic cells. (**A**) Representative contour plots showing TCRβ^+ CD4$^+$ cells gated on H-2Kd$^-$ cells from WT and *Tnxb*$^{-/-}$ mice, with or without stimulation. Percentages of TCRβ^+ CD4$^+$ cells among H-2Kd$^-$ cells were calculated in the columns with mean ± SD. (**B**) Representative contour plots showing TCRβ^+ CD8$^+$ cells gated on H-2Kd$^-$ cells from WT and *Tnxb*$^{-/-}$ mice, with or without stimulation. Percentages of TCRβ^+ CD8$^+$ cells among H-2Kd$^-$ cells were calculated in the columns with mean ± SD. Each group consisted of three mice ($n = 3$). ***$P < 0.001$; ****$P < 0.0001$; ns, not significant; one-way ANOVA followed by the Tukey test. (**C**) Representative contour plots showing CD69$^+$ CD4$^+$ cells gated on H-2Kd$^-$ TCRβ^+ cells from WT and *Tnxb*$^{-/-}$ mice. Percentages of CD69$^+$ CD4$^+$ cells among H-2Kd$^-$ TCRβ^+ cells were calculated in the columns with mean ± SD. (**D**) Representative contour plots showing CD69$^+$ CD8$^+$ cells gated on H-2Kd$^-$ TCRβ^+ cells from WT and *Tnxb*$^{-/-}$ mice. Percentages of CD69$^+$ CD8$^+$ cells among H-2Kd$^-$ TCRβ^+ cells were calculated in the columns with mean ± SD. Each group consisted of three mice (n=3). ***$P < 0.001$, two-tailed unpaired t test. H-2Kd$^-$, H-2Kd negative; TCRβ, T cell receptor β chain; CD69, T cell activation marker; stim., stimulation. The experiments are performed at least twice for reproducibility.

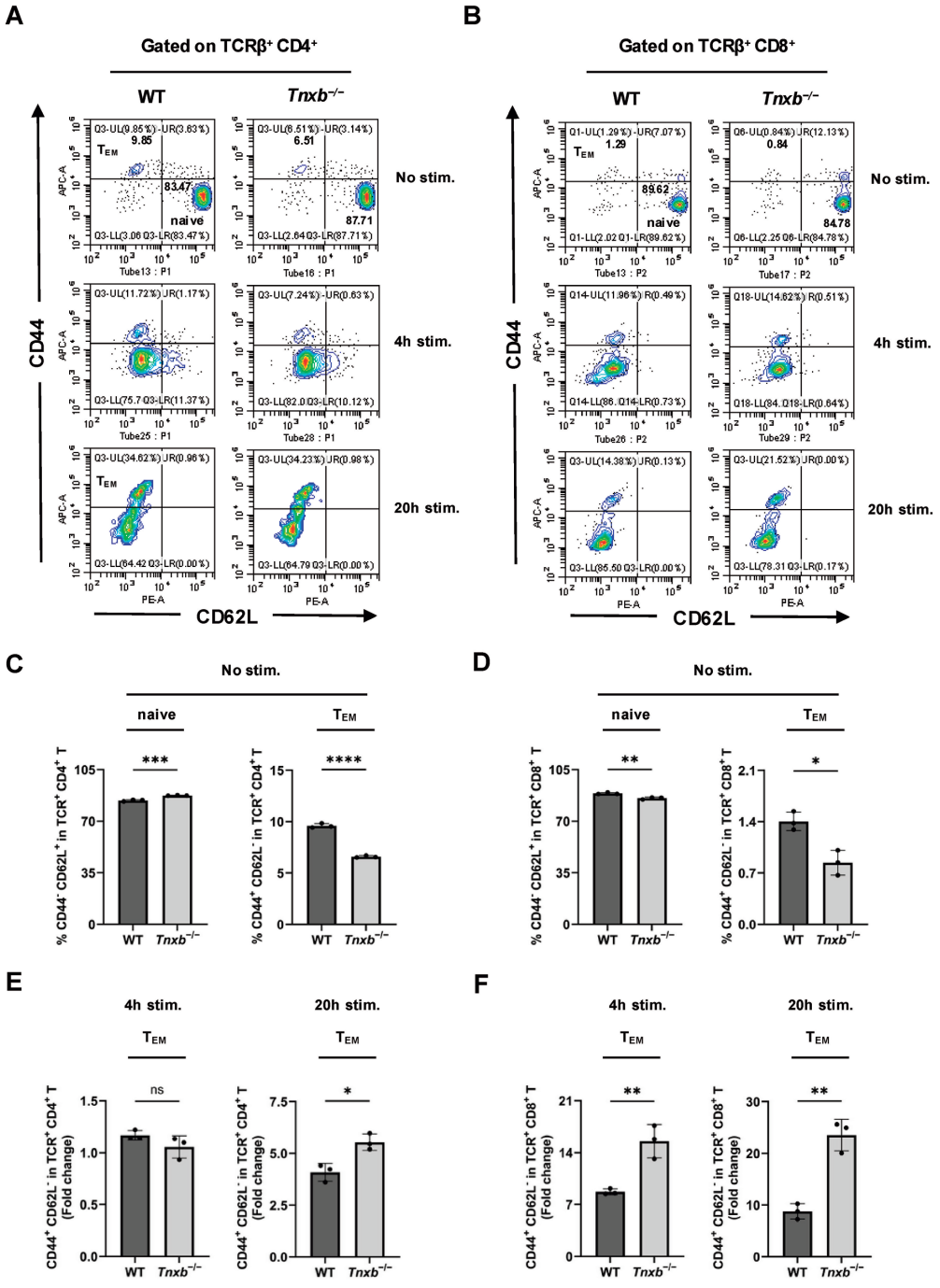

Fig. 4 CD4$^+$ and CD8$^+$ T cells from *Tnxb*$^{-/-}$ mice were more readily activated than those from WT mice. Phorbol myristate acetate (PMA) (40 ng/mL) and ionomycin (4 μg/mL) were added to the cell culture medium as stimulators for 4 h and 20 h. (**A**) Representative contour plots showing CD44$^-$ CD62L$^+$ T cells (naïve T cells) and CD44$^+$ CD62L$^-$ T cells (effector memory T cells, T_{EM}) gated on TCRβ^+ CD4$^+$ cells from WT and *Tnxb*$^{-/-}$ mice. (**B**) Representative contour plots showing CD44$^-$ CD62L$^+$ T cells (naïve T cells) and CD44$^+$ CD62L$^-$ T cells (T_{EM}) gated on TCRβ^+ CD8$^+$ cells from WT and *Tnxb*$^{-/-}$ mice. (**C**) Percentages of CD44$^-$ CD62L$^+$ T cells (naïve T cells) and CD44$^+$ CD62L$^-$ T cells (T_{EM}) among TCRβ^+ CD4$^+$ cells were calculated in the columns with mean ± SD. (**D**) Percentages of CD44$^-$ CD62L$^+$ T cells (naïve T cells) and CD44$^+$ CD62L$^-$ T cells (T_{EM}) among TCRβ^+ CD8$^+$ cells were calculated in the columns with mean ± SD. (**E**, **F**) CD4$^+$ and CD8$^+$ effector memory T cell populations that were normalized to the unstimulated control were calculated in the columns with mean ± SD after the stimulation at 4 h and 20 h. Each group consisted of three mice ($n = 3$). *$P < 0.05$; **$P < 0.01$; ***$P < 0.001$; ****$P < 0.0001$; ns, not significant; two-tailed unpaired *t* test. T_{EM}, effector memory T cells; TCRβ, T cell receptor β chain; stim., stimulation. The experiments are performed at least twice for reproducibility.

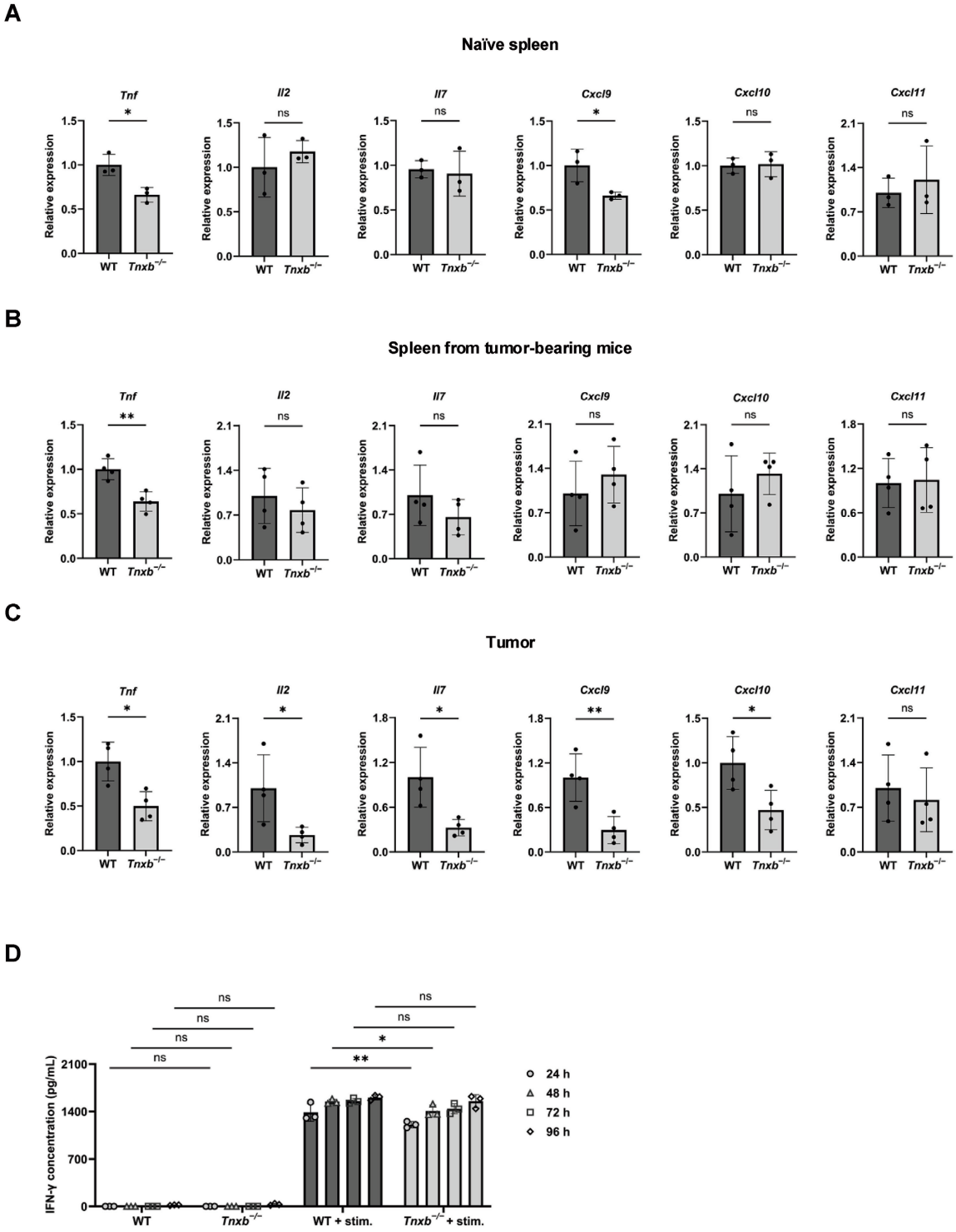

Fig. 5 The expression of T cell activation-related cytokines and chemokines in WT and *Tnxb*$^{-/-}$ mice with or without tumor inoculation. Relative mRNA expression of cytokines and chemokines in naïve spleens ($n = 3$) (**A**) and in spleens from tumor-bearing mice ($n = 4$) (**B**) and tumor tissues ($n = 4$) (**C**) was analyzed by RT-qPCR. Spleens and tumor tissues from tumor-bearing mice were harvested after the tumor inoculation at 12 days. Data were normalized to *Actb*. Data are expressed as mean ± SD (*$P < 0.05$; **$P < 0.01$; ns, not significant; two-tailed unpaired *t* test). (**D**) IFN-γ concentration was measured by ELISA assay after the stimulation with PMA and ionomycin at 24 h, 48 h, 72 h, and 96 h. Each group consisted of three mice ($n = 3$). Data are expressed as mean ± SD (*$P < 0.05$; **$P < 0.01$; ns, not significant; two-way ANOVA with uncorrected Fisher's LSD test). IFN-γ, Interferon-γ; stim., stimulation.

days (Fig. 6). CD45 and CD3 were used for leukocyte and T cell identification, respectively, whereas CD69 was used to assess T cell activation. In the naïve spleens, infiltrated $CD4^+$ and $CD8^+$ T cells were defined as $CD4^+$ $CD8^-$ and $CD4^-$ $CD8^+$, respectively, after gating on $CD45^+$ $CD3^+$ cells in the spleen (Supplementary Fig. 3A). The populations of $CD4^+$ and $CD8^+$ T cells, especially $CD8^+$ T cells, were reduced in *Tnxb*$^{-/-}$ mice than in WT mice (Supplementary Fig. 3B). These results indicate that the poor immune response traits of *Tnxb*$^{-/-}$ mice are intrinsic and present before tumor inoculation. In tumor tissues after tumor inoculation for 12 days, infiltrated $CD4^+$ and $CD8^+$ T cells were defined as $CD4^+$ $CD8^-$ and $CD4^-$ $CD8^+$, respectively, and activated $CD4^+$ and $CD8^+$ T cells as $CD69^+$ $CD4^+$ and $CD69^+$ $CD8^+$, respectively, after gating on $TCR\beta^+$ cells in tumors. $CD8^+$ T cell populations and activation were significantly lower in *Tnxb*$^{-/-}$ mice than in WT mice *in vivo*, while $CD4^+$ T cell populations and activation were not significantly (Fig. 6A and B). Meanwhile, immunofluorescence staining images revealed reduced infiltration of $CD4^+$ and $CD8^+$ T cells in the tumor tissues of *Tnxb*$^{-/-}$ mice compared with WT mice (Fig. 6C). These results indicate that TNXB deficiency reduced the number of infiltrating $CD8^+$ T cells in tumor tissues and impaired the activation of $CD8^+$ T cells *in vivo*.

DISCUSSION

TNXB, a key member of the tenascin family, is a crucial ECM glycoprotein. *TNXB* deficiency in humans causes a connective tissue disorder, clEDS1 (Malfait *et al.* 2020). Recent studies suggested that TNXB expression serves as a potential cancer biomarker (Liot *et al.* 2020; Matsumoto *et al.* 2020). We previously reported that TNXB acts as a tumor suppressor (Okuda-Ashitaka *et al.* 2023). In the present study, we demonstrated that TNXB deficiency promotes tumor progression by downregulating T cell activation-related cytokines and chemokines within the TME and reducing $CD8^+$ T cell infiltration and activation. These findings indicate that TNXB deficiency facilitates tumor progression and creates poor immune response in TME.

The tumor ECM affects the TME. As the most important noncellular component of the TME, the ECM regulates immune cell functions, such as migration, activation, proliferation, and differentiation, thereby reshaping the TME (Sorokin 2010). Changes in ECM components are considered as key factors in tumor progression (Huang *et al.* 2021; Yuan *et al.* 2023; Lee *et al.* 2024). Because TNXB expression is frequently downregulated in most tumor tissues (Liot *et al.* 2020), we first examined whether TNXB deficiency promoted tumor growth. As shown in Fig. 1A and B, *Tnxb*$^{-/-}$ mice exhibited significantly accelerated tumor growth and a poor survival rate after the tumor inoculation compared with WT mice. These results are consistent with those of our previous study (Matsumoto *et al.* 2001). Interestingly, Liot *et al* (2020) reported that TNXB downregulation is correlated with tumor progression, which further indicates that TNXB has a tumor suppressor role, and that a decrease in TNXB levels could promote tumor growth.

Tumor immunity relies heavily on T cells to effectively target and eliminate cancer cells (Waldman *et al.* 2020). Cytotoxic $CD8^+$ T cells are the primary killers of tumor cells, while $CD4^+$ T cells are involved in a pivotal role in maintaining responses of $CD8^+$ T cells and preventing their exhaustion (Raskov *et al.* 2021). TNXB is primarily expressed in fibroblasts in connective tissues, while its expression is low in immune tissues (Geffrotin *et al.* 1995); however, no relevant studies have explored the expression of TNXB in immune cells. In this study, we enriched T cells with nylon wool fiber and examined their *Tnxb* expression by RT-qPCR. We found that T cells did not express *Tnxb* (Fig. 2B) and possible *Tnxb*-expressed cells might be myeloid leukocytes, macrophages, and myeloid cells according to the single cell database analysis (Supplementary Fig. 1). These findings suggest that TNXB contributes externally to T cells in the TME.

T cell proliferation and differentiation are sophisticated, characterized by various signals against tumor growth and a healthy immune response (Zhang *et al.* 2005; Ahmed *et al.* 2022). *Tnxb*$^{-/-}$ mice exhibited significantly reduced $CD4^+$ and $CD8^+$ T cell populations after stimulation with allogeneic cells compared with those of WT mice (Fig. 3A and B). This finding *in vitro* is consistent with the finding of a reduced number of infiltrating $CD8^+$ T cells in tumor tissues of *Tnxb*$^{-/-}$ mice (Fig. 6A and C). However, unexpectedly, T cell activation from *Tnxb*$^{-/-}$ mice was significantly increased *in vitro*, especially for $CD4^+$ T cells after stimulation with allogeneic cells (Fig. 3C) and for $CD4^+$ and $CD8^+$ T cells after stimulation with PMA and ionomycin (Fig. 4E and F). This *in vitro* finding is inconsistent with the finding of decreased activation of infiltrating $CD8^+$ T cells in tumor tissues of *Tnxb*$^{-/-}$ mice (Fig. 6B). This discrepancy may be because although T cells of *Tnxb*$^{-/-}$ mice are more easily activated than those of

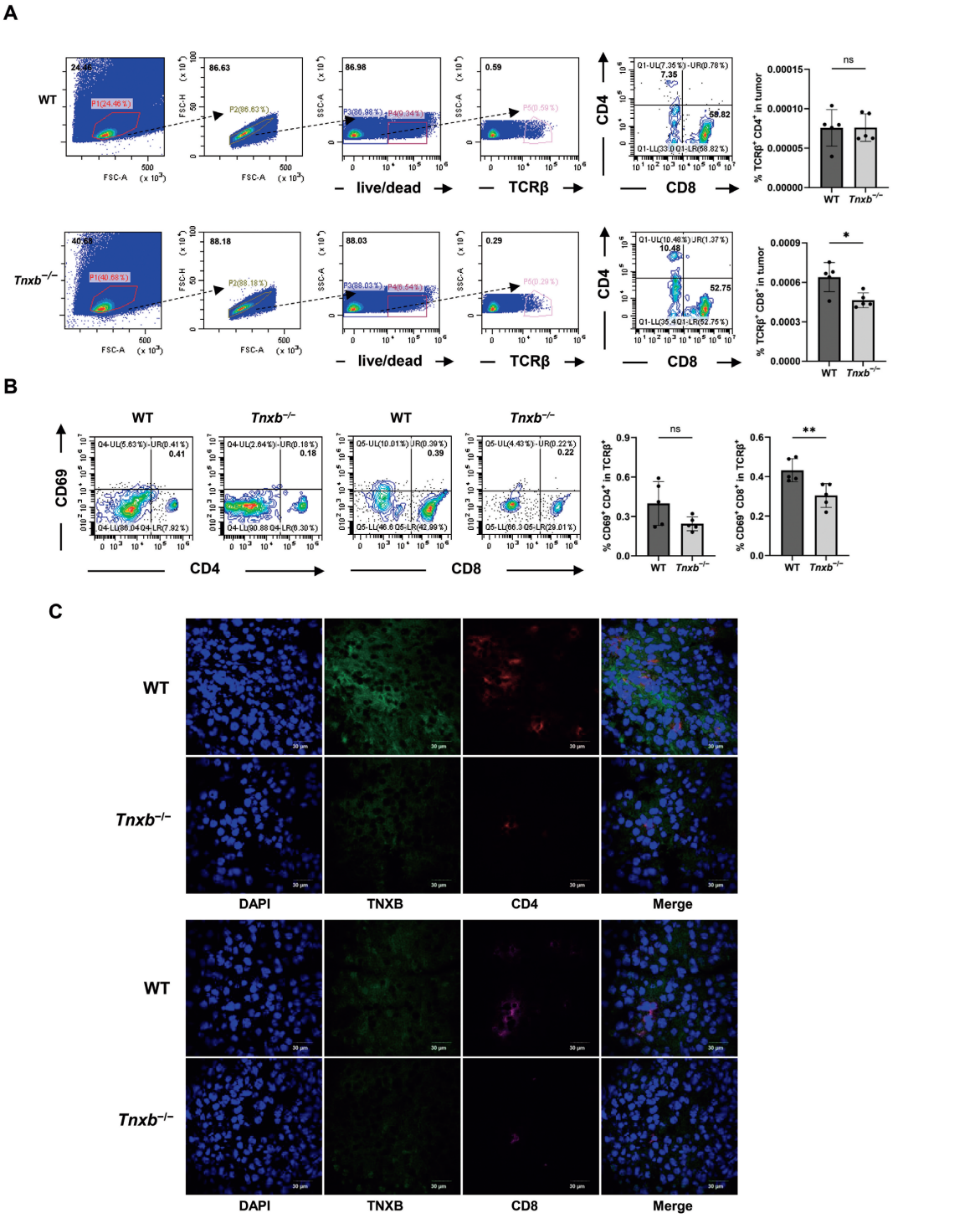

Fig. 6 Infiltration and activation of CD8$^+$ T cells were decreased in tumor tissues of *Tnxb*$^{-/-}$ mice. (**A**) Representative dot and contour plots showing CD4$^+$ CD8$^-$ and CD4$^-$ CD8$^+$ cells gated on TCRβ^+ cells in tumors from WT and *Tnxb*$^{-/-}$ mice. Relative population of TCRβ^+ CD4$^+$ or CD8$^+$ cells in tumor were calculated in the columns with mean ± SD. (**B**) Representative contour plots showing CD69$^+$ CD4$^+$ and CD69$^+$ CD8$^+$ cells gated on TCRβ^+ cells from WT and *Tnxb*$^{-/-}$ mice. Percentages of CD69$^+$ CD4$^+$ and CD69$^+$ CD8$^+$ cells among TCRβ^+ cells were calculated in the columns with mean ± SD. Each group contained five mice ($n = 5$). *$P < 0.05$; **$P < 0.01$; ns, not significant; two-tailed unpaired *t* test. TCRβ, T cell receptor β chain; CD69, T cell activation marker. (**C**) Representative immunofluorescence staining of tumor sections from WT and *Tnxb*$^{-/-}$ mice after tumor inoculation at 12 days ($n = 3$). Tumor sections were stained with antibodies: TNXB (green), CD4 (red), CD8 (purple), and 4',6-Diamidino-2-phenylindole (DAPI) (blue). Objective lens, 60×; scale bar, 30 μm.

WT mice *in vitro*, considering the decreased infiltrating $CD8^+$ T cells in tumor tissues, $Tnxb^{-/-}$ mice showed decreased levels of total activated infiltrating $CD8^+$ T cells in tumor tissues *in vivo*. Although $CD4^+$ and $CD8^+$ T cells were more activated in $Tnxb^{-/-}$ mice than in WT mice *in vitro* (Fig. 4E and F), IFN-γ concentration was significantly lower in the cell culture supernatant of $Tnxb^{-/-}$ mice than that of WT mice after 24 h and 48 h of stimulation (Fig. 5D). This may be due to the low expression of *Il2* and *Il7*, which are involved in immune cell proliferation and response in *in vitro* analysis.

Moreover, even before tumor inoculation, naïve spleens of $Tnxb^{-/-}$ mice exhibited a significantly downregulation of genes involved in immune inflammation and activation, such as *Tnf* and *Cxcl9* (Fig. 5A), and the upregulation of T cell exhaustion and suppressive markers, such as *Pdcd1*, *Ctla4* and *Ly6g* (Supplementary Fig. 2A). Furthermore, the relative populations of $CD8^+$ T cells were reduced in the naïve spleens of $Tnxb^{-/-}$ mice (Supplementary Fig. 3B). These results indicate that the poor immune response traits of $Tnxb^{-/-}$ mice are intrinsic and present even before tumor inoculation.

TNXB-deficient patients develop clEDS1 (Malfait *et al.* 2020). TNXB modulates the spacing between collagen fibrils via direct interaction with collagen molecules and collagen fibril-interacting molecules such as decorin (Valcourt *et al.* 2015). Electron microscopy has revealed increased inter-fibrillar distance between collagen fibrils in the connective tissues of patients with clEDS1 (Bristow *et al.* 2005). $CD8^+$ T cells can easily migrate in the stromal regions of a loose network of collagens (Salmon *et al.* 2012). Therefore, we initially anticipated that $Tnxb^{-/-}$ mice would exhibit increased infiltration of T cells into the TME than WT mice, but we found that the infiltration of T cells into the TME was decreased in $Tnxb^{-/-}$ mice. The explanation for the decrease in $CD8^+$ T cell infiltration into the TME due to TNXB deficiency remains unclear. Currently, clEDS1 patients with tumors are rarely diagnosed. In the future, it will be intriguing to examine morbidity and tumor progression in cancer patients with clEDS1.

In this study, we demonstrated that tumor progression in $Tnxb^{-/-}$ mice is caused by reducing $CD8^+$ T cell infiltration and its activation in the TME owing to decreased expression of T cell activation-related cytokines and chemokines and increased expression of T cell exhaustion and MDSC markers. However, the underlying molecular mechanism by which TNXB deficiency causes reduced $CD8^+$ T cell infiltration and alterations in cytokine and chemokine expression remains to be elucidated. Therefore, it is necessary to clarify this phenomenon at the molecular level. In addition, because TNXB suppresses tumor progression, the present study further underscores that TNXB within the TME could serve as a novel therapeutic target and an important regulator of anti-tumor immunity.

In conclusion, we demonstrated that TNXB deficiency causes tumor progression by reducing $CD8^+$ T cell infiltration and activation in the TME. Additionally, the poor immune response traits of $Tnxb^{-/-}$ mice are intrinsic and present even before tumor inoculation. This may be attributed to the reduced level of T cell activation-related cytokines and chemokines in $Tnxb^{-/-}$ mice. Our study provides new insights relevant to tumor control, immune response mediated by TNXB. Further studies are required to elucidate the precise molecular mechanisms by which TNXB influences immune cell infiltration and activation. Evidence that TNXB suppresses tumor progression warrants further investigation.

Acknowledgements

Author AG expresses gratitude to the Otsuka Toshimi Scholarship Foundation for its support and care during the Ph.D. course from 2023 to 2025 (Nos. 23-S94, 24-S79, and 25-S113). We also acknowledge the technical expertise of the Interdisciplinary Center for Science Research, Head Office for Research and Academic Information, Shimane University. This work was supported in part by the Management Expenses Grants of Shimane University to KM and YI.

CONFLICT OF INTEREST (COI)

The authors have declared no conflict of interest.

REFERENCES

Ahmed H, Mahmud AR, Siddiquee MF, Shahriar A, Biswas P, *et al.* (2022) Role of T cells in cancer immunotherapy: Opportunities and challenges. *Cancer Pathog Ther* **1**, 116–126.

Brellier F and Chiquet-Ehrismann R (2012) How do tenascins influence the birth and life of a malignant cell?. *J Cell Mol Med* **16**, 32–40.

Bristow J, Carey W, Egging D and Schalkwijk J (2005) Tenascin-X, collagen, elastin, and the Ehlers-Danlos syndrome. *Am J Med Genet C Semin Med Genet* **139C**, 24–30.

Chakravarthy A, Khan L, Bensler NP, Bose P and De Carvalho DD (2018) TGF-β-associated extracellular matrix genes link cancer-associated fibroblasts to immune evasion and immunotherapy failure. *Nat Commun* **9**, 4692.

Chiquet-Ehrismann R and Tucker RP (2011) Tenascins and the importance of adhesion modulation. *Cold Spring Harb Perspect Biol* **3**, a004960.

Demirdas S, Dulfer E, Robert L, Kempers M, van Beek D, *et al.* (2017) Recognizing the tenascin-X deficient type of Ehlers-Danlos syndrome: a cross-sectional study in 17 patients. *Clin Genet* **91**, 411–425.

Eble JA and Niland S (2019) The extracellular matrix in tumor progression and metastasis. *Clin Exp Metastasis* **36**, 171–198.

Geffrotin C, Garrido JJ, Tremet L and Vaiman M (1995) Distinct tissue distribution in pigs of tenascin-X and tenascin-C transcripts. *Eur J Biochem* **231**, 83–92.

Hanahan D and Coussens LM (2012) Accessories to the crime: functions of cells recruited to the tumor microenvironment. *Cancer Cell* **21**, 309–322.

Huang J, Zhang L, Wan D, Zhou L, Zheng S, *et al.* (2021) Extracellular matrix and its therapeutic potential for cancer treatment. *Signal Transduct Target Ther* **6**, 153.

Kuczek DE, Larsen AMH, Thorseth ML, Carretta M, Kalvisa A, *et al.* (2019) Collagen density regulates the activity of tumor-infiltrating T cells. *J Immunother Cancer* **7**, 68.

Lee CJ, Jang TY, Jeon SE, Yun HJ, Cho YH, *et al.* (2024) The dysadherin/MMP9 axis modifies the extracellular matrix to accelerate colorectal cancer progression. *Nat Commun* **15**, 10422.

Liot S, Aubert A, Hervieu V, Kholti NE, Schalkwijk J, *et al.* (2020) Loss of tenascin-X expression during tumor progression: A new pan-cancer marker. *Matrix Biol Plus* **6–7**, 100021.

Livak KJ and Schmittgen TD (2001) Analysis of relative gene expression data using real-time quantitative PCR and the $2^{-\Delta\Delta CT}$ Method. *Methods* **25**, 402–408.

Malfait F, Castori M, Francomano CA, Giunta C, Kosho T, *et al.* (2020) The Ehlers-Danlos syndromes. *Nat Rev Dis Primers* **6**, 64.

Matsumoto K, Takayama N, Ohnishi J, Ohnishi E, Shirayoshi Y, *et al.* (2001) Tumour invasion and metastasis are promoted in mice deficient in tenascin-X. *Genes Cells* **6**, 1101–1111.

Matsumoto K, Minamitani T, Orba Y, Sato M, Sawa H, *et al.* (2004) Induction of matrix metalloproteinase-2 by tenascin-X deficiency is mediated through the c-Jun N-terminal kinase and protein tyrosine kinase phosphorylation pathway. *Exp Cell Res* **297**, 404–414.

Matsumoto K, Sato T, Oka S, Inokuchi J and Ariga H (2004) Comparison of the compositions of phospholipid-associated fatty acids in wild-type and extracellular matrix tenascin-X-deficient mice. *Biol Pharm Bull* **27**, 1447–1450.

Matsumoto K, Kinoshita T, Hirose T and Ariga H (2006) Characterization of mouse serum tenascin-X. *DNA Cell Biol* **25**, 448–456.

Matsumoto K and Aoki H (2020) The roles of tenascins in cardiovascular, inflammatory, and heritable connective tissue diseases. *Front Immunol* **11**, 609752.

Murdamoothoo D, Sun Z, Yilmaz A, Riegel G, Abou-Faycal C, *et al.* (2021) Tenascin-C immobilizes infiltrating T lymphocytes through CXCL12 promoting breast cancer progression. *EMBO Mol Med* **13**, e13270.

Okuda-Ashitaka E and Matsumoto K (2023) Tenascin-X as a causal gene for classical-like Ehlers-Danlos syndrome. *Front Genet* **14**, 1107787.

Pickup MW, Mouw JK and Weaver VM (2014) The extracellular matrix modulates the hallmarks of cancer. *EMBO Rep* **15**, 1243–1253.

Raskov H, Orhan A, Christensen JP and Gögenur I (2021) Cytotoxic $CD8^+$ T cells in cancer and cancer immunotherapy. *Br J Cancer* **124**, 359–367.

Salmon H, Franciszkiewicz K, Damotte D, Dieu-Nosjean MC, Validire P, *et al.* (2012) Matrix architecture defines the preferential localization and migration of T cells into the stroma of human lung tumors. *J Clin Invest* **122**, 899–910.

Sorokin L (2010) The impact of the extracellular matrix on inflammation. *Nat Rev Immunol* **10**, 712–723.

Spenlé C, Saupe F, Midwood K, Burckel H, Noel G, *et al.* (2015) Tenascin-C: Exploitation and collateral damage in cancer management. *Cell Adh Migr* **9**, 141–153.

Spenlé C, Loustau T, Murdamoothoo D, Erne W, Beghelli-de la Forest Divonne S, *et al.* (2020) Tenascin-C orchestrates an immune-suppressive tumor microenvironment in oral squamous cell carcinoma. *Cancer Immunol Res* **8**, 1122–1138.

Tucker RP and Degen M (2019) The expression and possible functions of tenascin-W during development and disease. *Front Cell Dev Biol* **7**, 53.

Valcourt U, Alcaraz LB, Exposito JY, Lethias C and Bartholin L (2015) Tenascin-X: beyond the architectural function. *Cell Adh Migr* **9**, 154–165.

Waldman AD, Fritz JM and Lenardo MJ (2020) A guide to cancer immunotherapy: from T cell basic science to clinical practice. *Nat Rev Immunol* **20**, 651–668.

Yang N, Tian J, Wang X, Mei S, Zou D, *et al.* (2020) A functional variant in TNXB promoter associates with the risk of esophageal squamous-cell carcinoma. *Mol Carcinog* **59**, 439–446.

Yuan Z, Li Y, Zhang S, Wang X, Dou H, *et al.* (2023) Extracellular matrix remodeling in tumor progression and immune escape: from mechanisms to treatments. *Mol Cancer* **22**, 48.

Zhang N, Hartig H, Dzhagalov I, Draper D and He YW (2005) The role of apoptosis in the development and function of T lymphocytes. *Cell Res* **15**, 749–769.

Supplementary Table 1 *Primer sequences used for reverse transcription-quantitative PCR (RT-qPCR)*

Target gene		Sequence (5′ - 3′)	Product length
Pdcd1	Forward	CGGTTTCAAGGCATGGTCAT	142 bp
	Reverse	TCAGAGTGTCGTCCTTGCTT	
Ctla4	Forward	TACCCACCGCCATACTTTGT	106 bp
	Reverse	CTGCGACAAGGATCCAAAGG	
Ly6g	Forward	CTTGTCACTGTGCCTGCAAC	140 bp
	Reverse	CCCTGAGCTCTTTCTGCACA	
Ccl17	Forward	AGGTCACTTCAGATGCTGCTC	94 bp
	Reverse	ACTCTCGGCCTACATTGGTG	
Ccl22	Forward	GACACCTGACGAGGACACA	162 bp
	Reverse	GCAGAGGGTGACGGATGTAG	

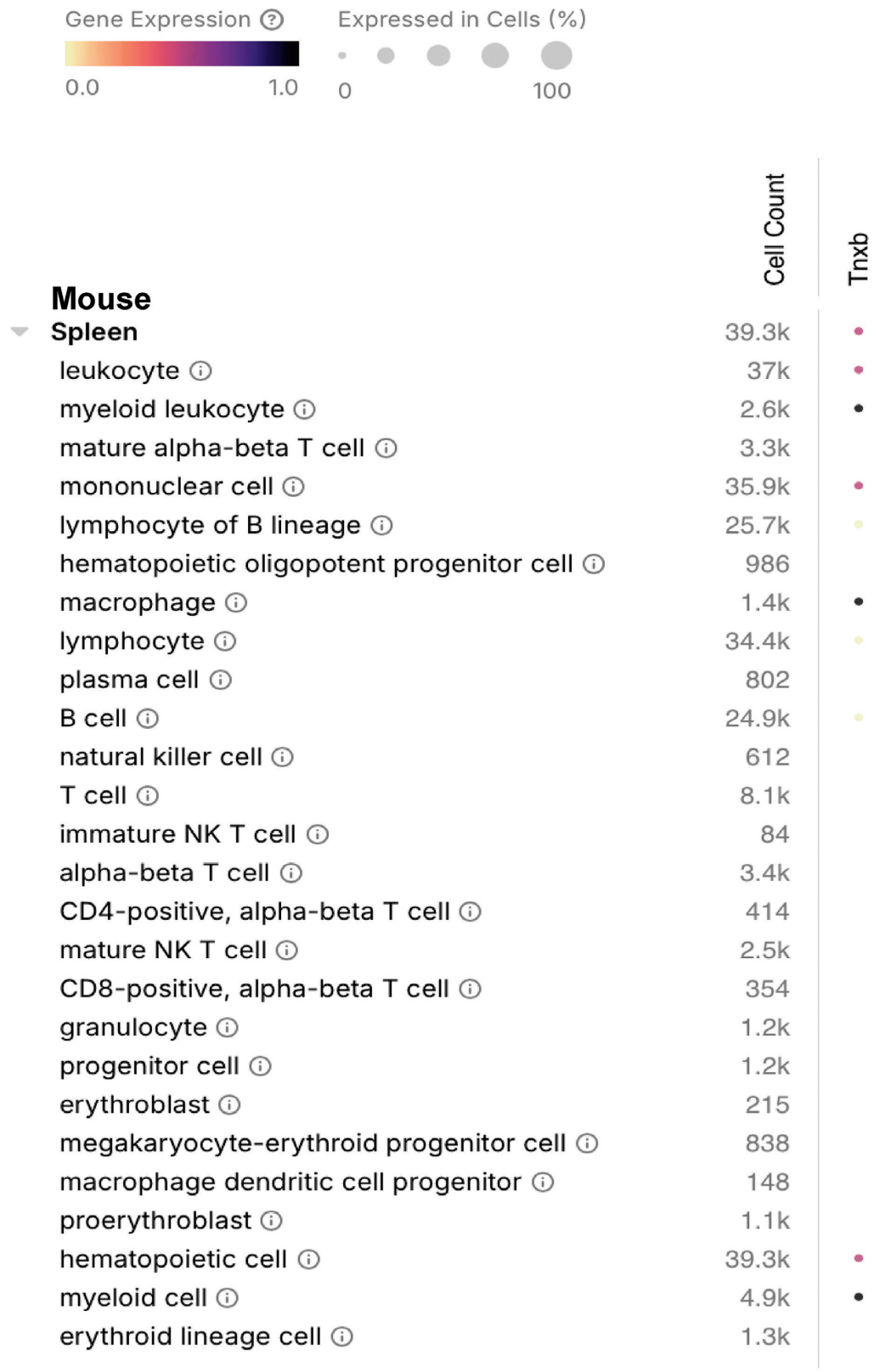

Supplementary Fig. 1 *Tnxb* is mainly expressed in myeloid leukocytes, macrophages, and myeloid cells but not in various types of T cells, according to the CZ CELLxGENE Discover single cell database analysis (https://cellxgene.cziscience.com).

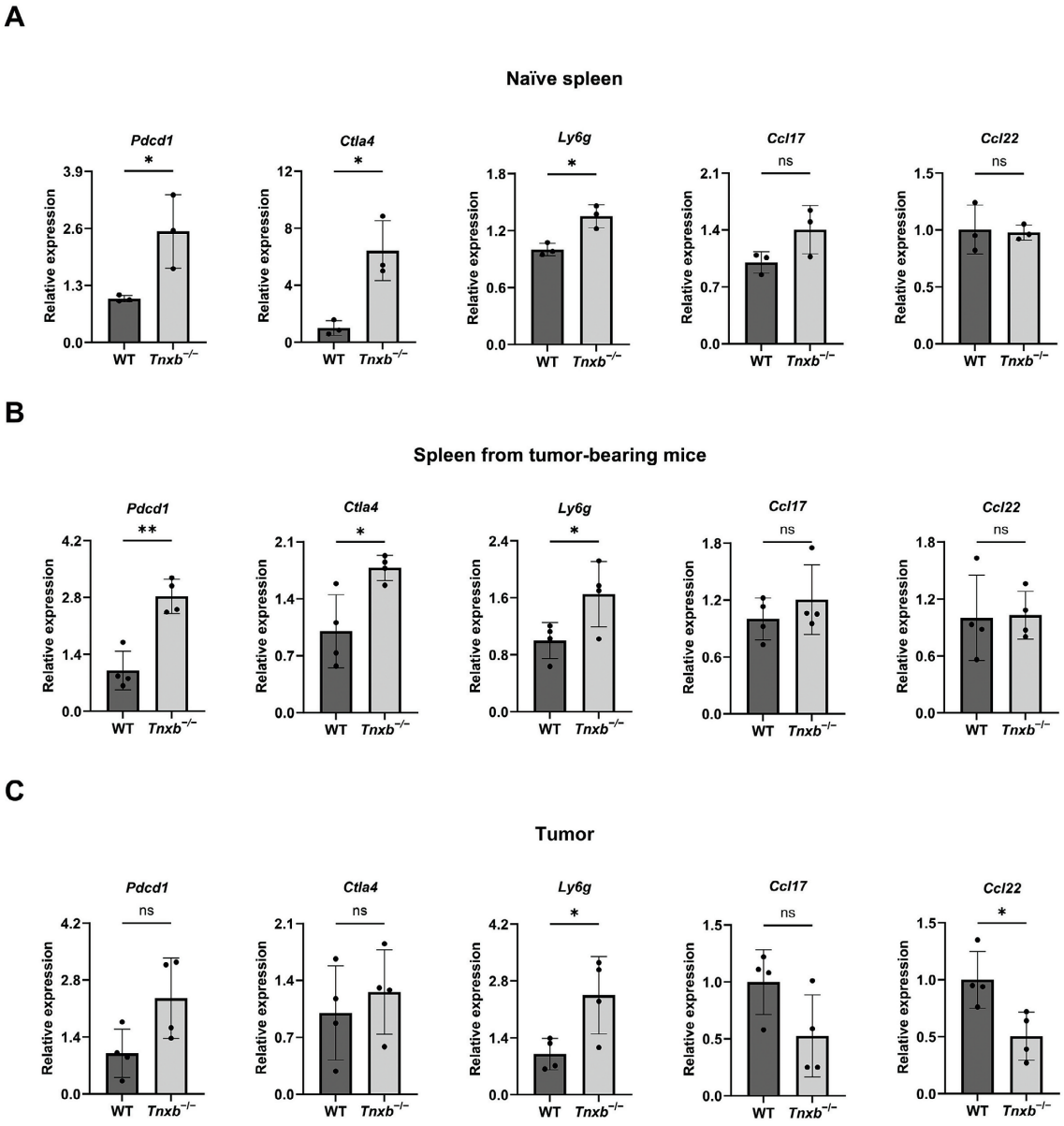

Supplementary Fig. 2 The expression of T cell activation-related cytokines and chemokines, and immune-related genes in WT and *Tnxb*$^{-/-}$ mice with or without tumor inoculation. Relative mRNA expression level of cytokines and chemokines, and immune-related genes in naïve spleens ($n = 3$) (**A**) and in spleen from tumor-bearing mice ($n = 4$) (**B**), and tumor tissue ($n = 4$) (**C**) was analyzed by RT-qPCR. Spleens and tumor tissues from tumor-bearing mice were harvested after tumor inoculation at 12 days. Data were normalized to *Actb*. Data are presented as mean ± SD (*$P < 0.05$; **$P < 0.01$; ns, not significant; two-tailed unpaired *t* test).

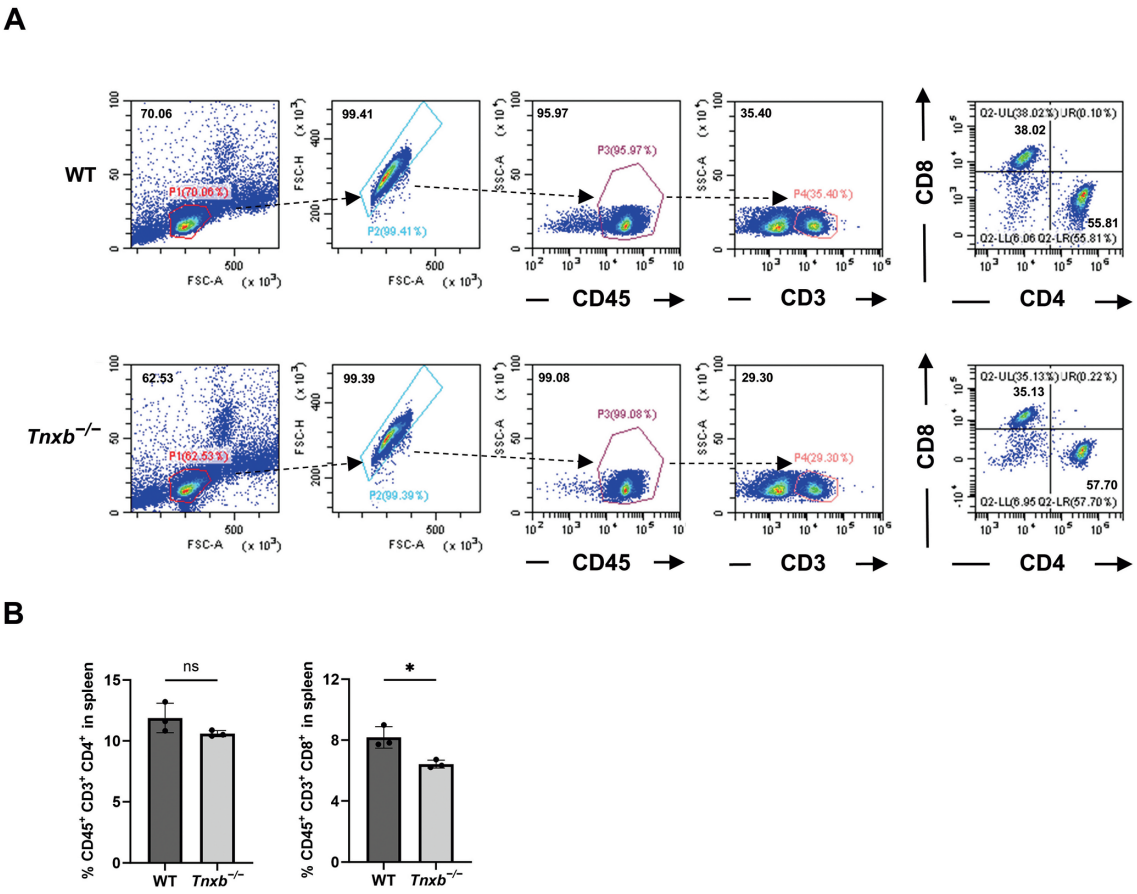

Supplementary Fig. 3 The populations of CD8$^+$ T cells were decreased in the naïve *Tnxb*$^{-/-}$ spleens. (**A**) Representative dot plots showing CD4$^+$ CD8$^-$ and CD4$^-$ CD8$^+$ cells gated on CD45$^+$ CD3$^+$ cells in spleen from WT and *Tnxb*$^{-/-}$ mice. (**B**) Relative population of CD45$^+$ CD3$^+$ CD4$^+$ or CD45$^+$ CD3$^+$ CD8$^+$ cells in spleens. Each group contained three mice ($n = 3$). *$P < 0.05$; ns, not significant; two-tailed unpaired *t*-test. CD45, leukocytes; CD3, T cells.